Available online at www.sciencedirect.com
ScienceDirect
Materials Chemistry and Physics 111 (2008) 209–212
MATERIALS CHEMISTRY AND PHYSICS
www.elsevier.com/locate/matchemphys

Crystal structure of dense nanocrystalline $BaTiO_3$ ceramics

C.J. Xiao [a,b,*], C.Q. Jin [b], X.H. Wang [c]

[a] *Department of Materials Science and Engineering, Henan University of Technology, Zhengzhou, China*
[b] *Institute of Physics, Chinese Academy of Science, Beijing 100080, China*
[c] *State Key Laboratory of New Ceramics and Fine Processing, Department of Materials Science and Engineering, Tsinghua University, Beijing, China*

Received 24 March 2007; received in revised form 21 November 2007; accepted 3 January 2008

Abstract

The dense nanocrystalline $BaTiO_3$ ceramics with the average grain size of 30 nm was sintered by the pressure assisted method. The Raman spectroscopy and the Rietveld refinement were employed to characterize the structural information of the nanocrystalline $BaTiO_3$ ceramics. The structural parameters and the reliability factors for the nanocrystalline $BaTiO_3$ ceramics were successfully determined by the Rietveld refinement based on the analysis of Raman spectra. A multiphase coexistence of tetragonal and orthorhombic phases was observed in 30 nm $BaTiO_3$ ceramics at room temperature. The phenomenon can be explained by the internal stress.

Keywords: Nanocrystalline ceramics; Crystal structure; Multiphase coexistence

1. Introduction

$BaTiO_3$ is one of the most widely used ferroelectric materials and has been extensively studied. It is a typical ABO_3 perovskite-type material with a variety of crystal structure modifications. Depending on the transition temperature, $BaTiO_3$ have five kinds of crystal systems, that is, hexagonal, cubic, tetragonal, orthorhombic and rhombohedral. For single-crystal and polycrystalline $BaTiO_3$, the phase transition temperatures are 1432, 130, 5 and −90 °C, respectively. Among them, the tetragonal phase is stable at room temperature. However, as the crystallite size of $BaTiO_3$ powder reduced to the nanoscale, some novel structural characters occurred [1–5]. For example, at room temperature, the cubic phase was observed and there is even a coexistence of hexagonal and tetragonal phases in $BaTiO_3$ nanoparticle with a size of 40 nm. In nanocrystalline $BaTiO_3$ ceramics, the different multiphase coexistences also occurred at various temperatures [6–8]. These phenomena indicated that the phase transition of $BaTiO_3$ may be a function of the temperature and the crystallite size. In order to investigate the properties of nanocrystalline $BaTiO_3$ ceramics, it is necessary to determine the crystal structure.

Although the size effects on the phase transition of $BaTiO_3$ were investigated, the structural studies have not been sufficiently carried out even though the structural data including lattice parameters, atomic positions, and phase fraction, are closely related to the ferroelectric properties. In particular, the quantitative structural information is more important to control the ferroelectric properties for nanocrystalline $BaTiO_3$ ceramics.

In this paper, based on the results of the Raman spectroscopy for the phase identification, we described in detail the structural study of nanocrystalline $BaTiO_3$ ceramics by means of the Rietveld refinement using X-ray powder diffraction data.

2. Experimental

The raw $BaTiO_3$ powder was synthesized by chemical processing [9]. The primary particle shape and size of raw $BaTiO_3$ powder was observed by the transmission electron microscopy (TEM). Fig. 1 showed the TEM micrograph of the raw $BaTiO_3$ powder. The TEM micrograph indicated that the average size of raw $BaTiO_3$ powder was about 10 nm and the overall shape was nearly spherical. In order to densify the sample and inhibit the grain growth, a three-step pressure assisted sintering was adopted. The raw $BaTiO_3$ powder was pressed into pellet uniaxially at 7 MPa. The pellet was cold pressed under 3 GPa at room temperature, then it was unloaded and ground into powder. The processed powder was repressed into pellet. The pellet was wrapped by Ag foil to prevent from contamination and then was inserted into BN spacer tube that was in turn put into the graphite heater. The high pressure sintering experiment was

* Corresponding author at: Department of Materials Science and Engineering, Henan University of Technology, Zhengzhou, China. Tel.: +86 371 67758740; fax: +86 371 67758721.
E-mail address: cjxiao@haut.edu.cn (C.J. Xiao).

0254-0584/$ – see front matter © 2008 Published by Elsevier B.V.
doi:10.1016/j.matchemphys.2008.01.020

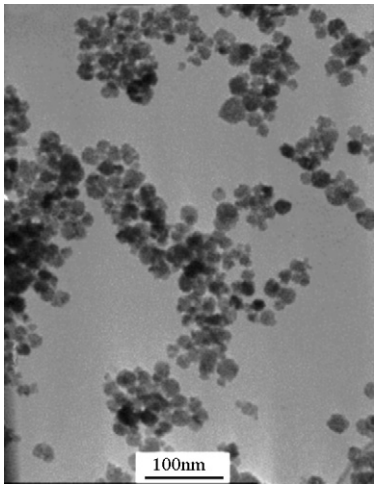

Fig. 1. TEM micrograph of 10 nm raw $BaTiO_3$ powder.

performed using a cubic anvil type apparatus. The pyrophyllite was used as the pressure-transmitting medium. The pellet was first pressurized up to 6 GPa and then heated at 1000 °C for 5 min in air. No sintering aids were added. After temperature quenching, the sample was obtained by releasing the pressure slowly to one atmospheric pressure.

The microstructure and grain size of $BaTiO_3$ ceramics was observed by scanning electron microscope (SEM, XL30-FEG) on fresh fracture surface. The Raman scattering, with the 633 nm lines of the exciting source from a He–Ne laser on a Renishaw RM2000 Confocal Raman Spectrometer, was used for the phase identification. The crystal structure of $BaTiO_3$ ceramics was refined by the Rietveld analysis of the X-ray diffraction (XRD) data, a pseudo-Voigt function was chosen as a profile function among profile ones. The XRD data were measured by scanning at intervals of 0.01° in the 2θ range from 10° to 140° using Cu Kα radiations with graphite monochromator on a Rigaku D/max-2500 diffractometry at room temperature.

3. Result and discussion

Fig. 2 showed the SEM image of $BaTiO_3$ ceramics. From the SEM image, the sample exhibits a uniform grain size distribution. The grain size was estimated to be about 30 nm by the intercept line method. The grain size was also calculated using Scherrer's equation from the full width at half maximum (FWHM) value of the broadening (1 1 1) reflection of XRD pattern taken for $BaTiO_3$ ceramics. The value of FWHM was 0.2874 and the grain size determined by the XRD method was about 28 nm. It was in agreement with the SEM result. Moreover, the sample was dense and the relative density was above 96% (theoretical density: 6.02 g cm^{-3}).

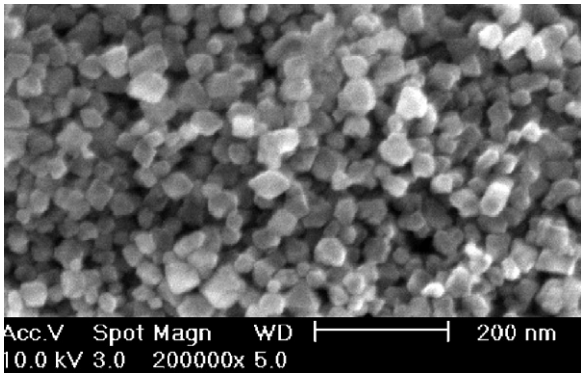

Fig. 2. SEM image of nanocrystalline $BaTiO_3$ ceramics with a grain size of 30 nm.

For single-crystal and polycrystalline $BaTiO_3$, the description of the Raman spectroscopy dependence on the temperature has been studied in 1965, and the detailed assignments of the vibrational frequencies have been carried out [10,11]. In addition, the evolution of Raman spectrum with decreasing grain size was characterized by an intensity decrease, a broadening of the line width, a frequency shift, and the disappearance of the Raman mode [12]. In nanocrystalline $BaTiO_3$ ceramics, the different multiphase coexistences at various temperatures were observed by Raman spectroscopy [6–8]. For 30 nm $BaTiO_3$ ceramics prepared by pressure assisted sintering, its crystal structure was also characterized by variable temperature Raman spectroscopy. Fig. 3 showed the Raman spectra of 30 nm $BaTiO_3$ ceramics at temperatures ranging from −190 to 200 °C. Because the grain size was reduced to the nanoscale, the intensity of Raman bands weakened, the line width broadened and the bands at near 487 cm^{-1} [E(TO)] and 715 cm^{-1} [A1(LO)] disappeared. Now, compared with that of the $BaTiO_3$ crystal, we discuss the evolution of Raman spectra of 30 nm $BaTiO_3$ ceramics with increasing temperature. At −190 °C, except for the bands disappearing at 487 and 715 cm^{-1}, the Raman spectra features are similar to those of $BaTiO_3$ crystal at the same temperature. So it is concluded to be a rhombohedral phase. With increasing temperature from −190 to −50 °C, the band at 167 cm^{-1} [A1(TO)] disappeared and the band at 184 cm^{-1} [A1(LO)] shifted to 187 cm^{-1}. These changes are indicative of the rhombohedral-to-orthorhombic phase transition. When the sample was heated to 50 °C, the most noticeable change is that the band at 187 cm^{-1} disappeared, which indicates the orthorhombic-to-tetragonal phase transition. At 25 °C, the frequencies of bands at 245 cm^{-1} [A1(TO)] and 306 cm^{-1} [B1, E(TO + LO)] are the same as those of at 50 °C and the band at 188 cm^{-1} still exists. So it is inferred that the orthorhombic and tetragonal phases coexist at room temperature. When fur-

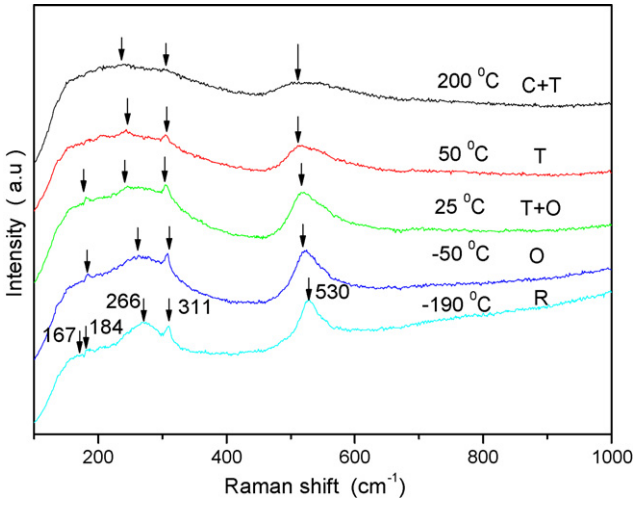

Fig. 3. Raman spectra of nanocrystalline $BaTiO_3$ ceramics at various temperatures. The different phases are marked as C, cubic; T, tetragonal; O, orthorhombic; and R, rhombohedral phase, respectively.

ther heated to 200 °C, two broader bands at 235 cm^{-1} [A1(TO)] and 515 cm^{-1} [A1(TO)] were still observed. This is mainly due to the broken translation symmetry by the boundaries, defects or by possible short-range polar order regions existing in the cubic state [6,11]. Moreover, a very weak band at 306 cm^{-1} [B1, E(TO + LO)] also persisted. So the dominant phase is cubic one. From the Raman analysis, it is clear that the coexistence of ferroelectric tetragonal and orthorhombic phases was observed in 30 nm $BaTiO_3$ ceramics at room temperature.

Although the different multiphase coexistences at various temperatures were observed by Raman spectroscopy in nanocrystalline $BaTiO_3$ ceramics [6–8], all the results were not confirmed by other method. In this paper, we employed the Rietveld refinement to identify the crystal structure of nanocrystalline $BaTiO_3$ ceramics. The Rietveld refinement requires an approximate structural model for the actual structure. The FullProf. Suite program was applied to refine the structural model. The initial Rietveld refinement was done by the zero-point shift, the unit-cell, and background parameters. After a good match, the peak position was achieved and the peak profile parameters including the peak asymmetry were refined. Firstly, we performed the Rietveld refinement based on the tetragonal and orthorhombic crystal systems, respectively. The final weighted *R*-factors, R_{wp} and the goodness of fit indicator, S (=R_{wp}/R_e) were 13.6%, 1.67 and 15.8%, 1.94, respectively. According to the Raman spectrum results, we tried to carry out the Rietveld refinement with the mixture phase model that contains both tetragonal and orthorhombic crystal systems. The same Rietveld refinement was applied to the mixture structural model. All *R*-factors for the mixture structural model were lower than those for the tetragonal and orthorhombic structures. The final weighted *R*-factors R_{wp} and the goodness of fit indicator, S (=R_{wp}/R_e) were decreased to 12.1% and 1.43, respectively. Fig. 4 showed the Rietveld refinement patterns of the mixture structural model, which contains a coexistence of tetragonal and orthorhombic phases. Table 1 gave the structural parameters obtained from the Rietveld refinement. From the Rietveld refinement results, the mass fractions of tetragonal and orthorhombic phases based

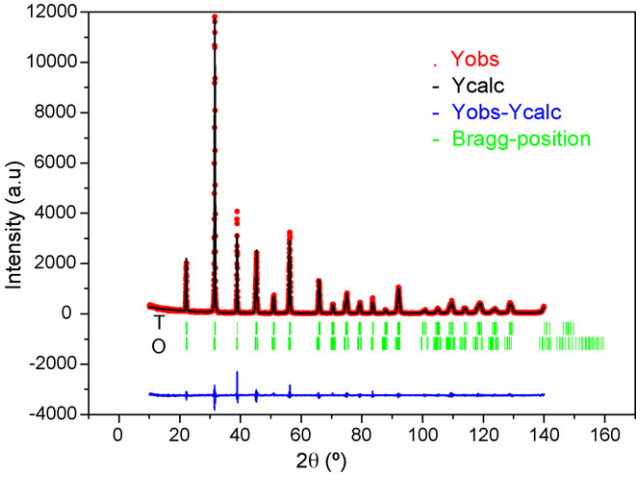

Fig. 4. The structural refinement patterns of $BaTiO_3$ using X-ray powder diffraction data for a mixture of tetragonal and orthorhombic phases.

Table 1
Structural parameters for 30 nm $BaTiO_3$ ceramics obtained from the structural refinement using X-ray powder diffraction data at room temperature

Symmetry and lattice parameters	Sites	Atomic coordinates			U_{iso} (Å^2)
		x	*y*	*z*	
T: *P4mm*	Ba	0.0	0.0	0.0	0.196(5)
$a = b = 3.9988(2)$ Å	Ti	0.5	0.5	0.5021(4)	0.018(8)
$c = 4.0222(4)$ Å	O1	0.5	0.5	−0.0153(6)	0.017(1)
$c/a = 1.0058$	O2	0.5	0.0	0.5130(3)	0.011(4)
O: *Amm2*	Ba	0.0	0.0	0.0	0.176(3)
$a = 4.0094(3)$ Å	Ti	0.5	0.0	0.5100(2)	0.016(1)
$b = 5.6214(9)$ Å	O1	0.0	0.5	0.4900(4)	0.045(7)
$c = 5.6386(3)$ Å	O2	0.5	0.7525(7)	0.7396(6)	0.028(2)

Phase fraction (%)

Tetragonal	Orthorhombic
66.3	33.7

on the refined scale factors for the two phases were 66.3% and 33.7%, respectively. The lattice parameters for each phase were a (=b) = 3.9988(2) Å, c = 4.0222(4) Å and a = 4.0094(3) Å, b = 5.6214(9) Å, c = 5.6386(3) Å, respectively. So it could conclude that this approach may be suitable to determine the structural parameters for the nanocrystalline $BaTiO_3$ ceramics, such as mass fractions, lattice parameters, atomic coordinates, and isotropic thermal parameters. The Rietveld refinement result supported that the 30 nm $BaTiO_3$ ceramics contained both tetragonal and orthorhombic phases.

The room-temperature stabilization of the cubic structure in fine-grained $BaTiO_3$ has been explained by two models: the phenomenological surface layer model [13,14] and the pure phase model. In the pure phase model, two mechanisms have been proposed to explain the room-temperature stabilization of the cubic structure. The first is concerned with the strain imposed by the presence of the lattice hydroxyl ions and the second is the role of surface effects [4]. In polycrystalline $BaTiO_3$ ceramics, the grains, which are surrounded by neighboring grains, are considered to be in a significantly different situation from individual powders of the same size. In an isolated particle, the atomic structure of nanostructure materials can differentiate between: (i) the core of the particle and (ii) free surface surrounding the core. In a constrained solid nanocrystal, such as in ceramics, there are: (iii) cores and (iv) grain boundaries [15]. For nanocrystalline ceramics, the macroscopic properties are dominated by the extrinsic effects exerted by the grain boundaries [16]. The coexistence of tetragonal and orthorhombic phases at room temperature in fine-grained $BaTiO_3$ ceramics was explained in terms of the internal stress at the grain boundaries. During the ferroelectric transition, the internal stress developed. In coarse-grained ceramics, the localized shear stress at the grain boundaries, which hindered the transition, can be relieved by formation of 90° domains. In fine-grained $BaTiO_3$ ceramics, when the grain size was below 300–500 nm, there is a reduced number of 90° domains and the single domain becomes energetically favorable [17–19], thus the stress cannot be relieved due to the absence of 90° domains [20,21]. In order to minimize strain

energy, twinning along {1 1 0} plane (90° twinning) took place in a constrained grain. Compared with the tetragonal structure, the unit-cell of orthorhombic structure, whose polar axis parallels to a face diagonal, i.e. (0 1 1) direction, was characterized by a shear deformation of the cubic perovskite cell. In terms of the stress-relieving twinning mechanisms, the orthorhombic structure can more efficiently minimize transition stress, so its stability is enhanced [1]. Therefore, at room temperature, the orthorhombic phase inclined to exist together with the tetragonal phase in nanocrystalline $BaTiO_3$ ceramics.

4. Conclusions

Through the combination of the Raman spectrum and the Rietveld refinement using X-ray powder diffraction data, the structural parameters for the nanocrystalline $BaTiO_3$ ceramics, such as mass fractions, lattice parameters, atomic coordinates, and isotropic thermal parameters, all were successfully determined. A multiphase coexistence of the tetragonal and orthorhombic phases was observed in 30 nm $BaTiO_3$ ceramics. The weight fractions were estimated to be 66.3% and 33.7%, respectively. The lattice parameters for the tetragonal phase were a (=b) = 3.9988(2) Å, c = 4.0222(4) Å and for the orthorhombic phase were a = 4.0094(3) Å, b = 5.6214(9) Å, c = 5.6386(3) Å, respectively.

Acknowledgements

This work is supported by the Ministry of Sciences and Technology of China through the 973-Project under Grant No. 2002CB613301.

References

[1] M.H. Frey, D.A. Payne, Phys. Rev. B 54 (1996) 3158.
[2] M. Yashima, T. Hoshina, D. Ishimura, S. Kobayashi, W. Nakamura, T. Tsurumi, S. Wada, J. Appl. Phys. 98 (2005) 014313.
[3] T. Yamamoto, K. Urabe, H. Banno, Jpn. J. Appl. Phys. 32 (1993) 4272.
[4] X. Li, W.-H. Shih, J. Am. Ceram. Soc. 80 (1997) 2844.
[5] B.D. Begg, E.R. Vance, J. Nowotny, J. Am. Ceram. Soc. 77 (1994) 3186.
[6] V. Buscaglia, M.T. Buscaglia, M. Viviani, T. Ostapchuk, I. Gregora, J. Petzelt, L. Mitoseriu, P. Nanni, A. Testino, R. Calderone, C. Harnagea, Z. Zhao, M. Nygren, J. Eur. Ceram. Soc. 25 (2005) 3059.
[7] X.Y. Deng, X.H. Wang, H. Wen, A.G. Kang, Z.L. Gui, L.T. Li, J. Am. Ceram. Soc. 89 (2006) 1059.
[8] G. Arlt, D. Hennings, G.D. With, J. Appl. Phys. 58 (1985) 1619.
[9] B.R. Li, X.H. Wang, L.T. Li, Mater. Chem. Phys. 78 (2002) 292.
[10] C.H. Perry, D.B. Hall, Phys. Rev. Lett. 15 (1965) 700.
[11] U.D. Venkateswaran, V.M. Naik, R. Naik, Phys. Rev. B 58 (1998) 14256.
[12] Y.L. Du, M.S. Zhang, Q. Chen, Z. Yin, Appl. Phys. A 76 (2003) 1099.
[13] S. Malbe, J.C. Mutil, J.C. Niepcc, J. Chim. Phys. 89 (1992) 825.
[14] J.C. Niepcc, in: L.C. Dufor (Ed.), Surfaces and Interfaces of Ceramics Materials, Kluwer Academic Publishers, 1989.
[15] B. Palosz, S. Gierlotka, S. Stel'makh, R. Pielaszek, P. Zinnb, M. Winzenickb, U. Bismayerc, H. Boysen, J. Alloys Compd. 286 (1999) 184.
[16] M.T. Buscaglia, M. Viviani, V. Buscaglia, L. Mitoseriu, A. Testino, P. Nanni, Z. Zhao, M. Nygren, C. Harnagea, D. Piazza, C. Galassi, Phys. Rev. B 73 (2006) 064114.
[17] Z. Zhao, V. Buscaglia, M. Viviani, M.T. Buscaglia, L. Mitoseriu, A. Testino, M. Nygren, M. Johnsson, P. Nanni, Phys. Rev. B 70 (2004) 024107.
[18] M.H. Frey, Z. Xu, P. Han, D.A. Payne, Ferroelectrics 206–207 (1998) 337.
[19] S.B. Ren, C.J. Lu, H.M. Shen, Y.N. Wang, Phys. Rev. B 55 (1997) 3485.
[20] G. Arlt, Ferroelectrics 104 (1990) 217.
[21] K. Kyoichi, A. Yamaji, J. Appl. Phys. 47 (1976) 371.